Space Weather

RESEARCH ARTICLE
10.1029/2019SW002325

Special Section:
Space Weather Events of 4-10 September 2017

Subauroral and Polar Traveling Ionospheric Disturbances During the 7–9 September 2017 Storms

Shun-Rong Zhang[1], Philip J. Erickson[1], Anthea J. Coster[1], William Rideout[1], Juha Vierinen[2], Olusegun Jonah[1], and Larisa P. Goncharenko[1]

[1]Haystack Observatory, Massachusetts Institute of Technology, Westford, MA, USA, [2]Department of Physics and Technology, University of Tromsø, Tromsø, Norway

Key Points:
- First evidence of storm time concurrent large and medium spatial scale traveling ionospheric disturbances at subauroral latitudes was reported
- Casual relation between medium-scale traveling ionospheric disturbances and the subauroral polarization stream were found
- Unexpected persistent transpolar day-to-night propagation of traveling ionospheric disturbances occurred

Correspondence to:
S.-R. Zhang,
shunrong@mit.edu

Citation:
Zhang, S.-R., Erickson, P. J., Coster, A. J., Rideout, W., Vierinen, J., Jonah, O. F., & Goncharenko, L. P. (2019). Subauroral and polar traveling ionospheric disturbances during the 7–9 September 2017 storms. *Space Weather*, *17*, 1748–1764. https://doi.org/10.1029/2019SW002325

Received 6 AUG 2019
Accepted 30 NOV 2019
Accepted article online 4 DEC 2019
Published online 25 DEC 2019

Abstract This study provides new scenarios for storm time traveling ionospheric disturbance excitation and subsequent propagation at subauroral and polar latitudes. We used ground-based total electron content observations from Global Navigation Satellite System receivers combined with wide field, subauroral ionospheric plasma parameters measured with the Millstone Hill Incoherent Scatter Radar during strong September 2017 geospace storms. Observations provide the first evidence of significant influences on traveling ionospheric disturbance (TID) propagation and excitation caused by the presence of large subauroral polarization stream flow channels. Simultaneous large- and medium-scale TIDs evolved during the event in a broad subauroral and midlatitude area near dusk. Similar concurrent TIDs occurred near dawn sectors as well during a period of sustained southward Bz. Medium-scale TIDs at subauroral and midlatitudes had wave fronts aligned northwest-southeast near dusk, and northeast-southwest near dawn. These wave fronts were highly correlated with the direction of storm time large zonal plasma drift enhancements at these latitudes. At high latitudes, unexpected, predominant, and persistent storm time TIDs were identified with 2000+ km zonal wave fronts and 15% total electron content perturbation amplitudes, moving in transpolar propagation pathways from the dayside into the nightside. This propagation direction in the polar region was opposite to the normal assumption that TIDs originated in the nightside auroral region. Results suggest that significant dayside sources, such as cusp regions, can be efficient in generating transpolar TIDs during geospace storm intervals.

Plain Language Summary This paper reports several new findings on the traveling ionospheric disturbances (TIDs) excited during geospace storms in 7–8 September 2017. Storm time TIDs provide pathway for momentum and energy dispersion from the solar wind-magnetosphere system to various components of the global ionosphere and thermosphere. Storm time large-scale TIDs (LSTIDs) have been identified by many studies as being initiated generally in the auroral zone where significant heating is injected, with subsequent propagation away from the source: equatorward into lower latitudes and poleward into high latitudes. Our study indicates that, during equatorward propagation, LSTIDs can encounter strong dynamic forcing at subauroral latitudes in the zonal direction. This westward velocity forcing is provided by a SAPS (subauroral polarization stream) channel and furthermore appears to be associated with the developing of medium-scale TIDs (MSTIDs). Thus, this paper provides the first causal link between these TIDs and SAPS flow channels. Concurrent LSTIDs and MSTIDs existed during the September storm in not only near dusk but also dawn sectors. In the polar cap region, conventionally anticipated poleward propagation away from the auroral zone was unexpectedly weak. In contrast, an opposite sense of transpolar propagation from the dayside into the nightside (i.e., equatorward at night and poleward during the day) was observed and furthermore was persistent and large in amplitude. This unexpected propagation may imply an efficient additional storm time source region of TID excitation at high latitudes on the dayside, for example, near the cusp. This study demonstrates that modern TID studies have continued potential for fresh insights into magnetosphere-ionosphere-thermosphere coupling processes.

1. Introduction

Traveling ionospheric disturbances (TIDs) are a ubiquitous and permanent feature of upper atmospheric variability and impose a primary challenge for accurate specification and prediction of the ionosphere and

thermosphere weather. Ionospheric-thermosphere (I/T) coupling forms the key generative process of TIDs. This coupling spans the excitation processes of atmospheric waves (e.g., acoustic gravity waves, AGWs), ionospheric instabilities (e.g., the Perkins instability, PI), the ionospheric manifestation of traveling atmospheric disturbances (TADs) or/and AGWs, and ionospheric feedback pathways to propagating neutral waves (e.g., through damping).

Classifying TIDs into different categories is important, since different scale sizes of TIDs imply the possibility of different excitation mechanisms and propagation properties. Large-scale TIDs (LSTIDs) have a typical horizontal velocity of 400–1,000 m/s, a 30- to 180-min period, and a horizontal wavelength of ≥1,000 km. Medium-scale TIDs (MSTIDs) form another disturbance wave class that are excited through quite many processes including the high-latitude disturbances. They have a typical horizontal velocity of 250–1,000 m/s, a 15- to 60-min period, a horizontal wavelength of several hundred kilometers. These features have been reviewed by several authors including Francis (1975), Hunsucker (1982), Yeh and Liu (1974), and Hocke and Schlegel (1996). Geospace disturbances encompass magnetic storms and substorms and other magnetosphere-ionosphere coupling phenomena, and these forcing events are well known as a primary excitation source of many LSTID/TAD/AGWs, due to such mechanisms as enhancements in Joule heating and particle heating driven by solar wind and magnetospheric energy, momentum, and material injection. It is very evident that storm time energy and momentum deposition at high latitudes can be transported by TIDs into higher altitudes and lower latitudes (Richmond, 1978; Yeh & Liu, 1974), subsequently driving significant regional or even global variations in the ionosphere and thermosphere system (Lu et al., 2015).

Many prior theoretical investigations have explored the AGW/TID excitation and propagation in the thermosphere and ionosphere (Lu et al., 2015; Richmond, 1978; Vadas & Nicolls, 2012). In particular, the propagation of internal AGWs is based on those well-defined dispersion and polarization relations (e.g., Hines, 1960), which describe how the atmospheric background parameters (neutral density, temperature and winds, and including their height gradients) determine the wave characteristics. Thus, the gravity wave (GW) oscillation frequency is always lower than the buoyancy Brunt-Väisälä frequency, which is dependent on the speed of sound; the neutral particle trajectory is always parallel to the phase line of the wave, and the phase line must tilt toward the propagating direction. Most of these wave characteristics are derived under the assumption that the ionosphere is merely responding to the propagation of those neutral waves and is set into motion, and accordingly, the waves are damped (e.g., Liu & Yeh, 1969). During geospace storms, however, strong ion-neutral coupling is known to significantly impact the neutral density, temperature, and winds in many ways, and the atmospheric medium is subject to dynamical changes on a global scale. When atmospheric waves propagate into regions such as subauroral latitudes where dramatic ionospheric electrodynamical processes take place with apparent thermospheric consequences, the changing and inhomogeneous atmospheric conditions and regional heating can modify these waves. In this work, we use Global Navigation Satellite System (GNSS) based total electron content (TEC) observations during the 7–8 September 2017 geospace storms to demonstrate some of these TID complexities, including a few unusual features that have not been reported previously.

In general, TID observations show important dynamic features that challenge understanding of their source and propagation, including multiple frequencies with varying spatial and temporal scale sizes, and trains of waves rather than a single impulse or few impulses. Furthermore, most prior storm time TID studies have focused on LSTIDs (see; Borries et al., 2009; Ding et al., 2007; Jonah et al., 2018; Zakharenkova et al., 2016), whereas the present work emphasizes TIDs with smaller periodicities primarily ≤30 min. They have shorter periods than typical LSTIDs with spatial scales varying from a few hundred kilometers up to at least 4,000 km.

The existence of this type of short period and large spatial scale TIDs has been previously reported predominately in the continental United States (CONUS), which has a densely distributed GNSS ground-based observational network. Tsugawa et al. (2007) reported MSTIDs for both nighttime conditions with 200–500 km wavelengths and wave front extent of 2,000 km, and for daytime conditions with 300–1,000 km wavelengths. All these TIDs appeared to be associated with geomagnetic disturbances. Lyons et al. (2019) studied various auroral-related nighttime TIDs derived using a 30-min sliding window detrending method, which by necessity emphasized oscillations at ≤30-min periods. The study also found ionospheric structures with >1,000 km large wave fronts and >500 km horizontal wavelengths. The present study uses data from both CONUS and Europe to place these class of TIDs into an even larger context. In the description that follows, we use LSSTID to represent these very large spatial scale TIDs whose periodicity is relatively short (≤30 min).

High-latitude magnetosphere-ionosphere coupling and heating processes are known to excite not only LSTIDs but also MSTIDs. Supersonic moving auroral electrojet arcs, for example, can excite MSTIDs (Hunsucker, 1982). These high-latitude MSTIDs are different in excitation mechanisms from typical nighttime MSTIDs often observed at middle and low latitudes under nonstorm conditions (Frissell et al., 2014; Kotake et al., 2007; Oinats et al., 2016; Shiokawa et al., 2003). In addition to AGWs, some nonstorm MSTIDs propagate southwestward, with excitation explained through invocation of the PI (Fukao et al., 1991; Otsuka et al., 2004; Perkins, 1973; Saito et al., 2001). While the extensively studied LSTIDs are easily observed due to their large spatial scales and large fluctuation amplitudes, MSTIDs associated with geospace storm and substorm activities are typically a regional phenomenon with limited spatial scales and small fluctuation amplitudes and are poorly known with few observations. In this study, we report subauroral MSTIDs that occurred concurrently with LSTIDs and were furthermore correlated to dynamic features specific to subauroral storm time response, and in particular to the existence of a fast zonal flow channel known as the subauroral polarization stream (SAPS; Foster & Burke, 2002). To our knowledge, this LSTID + MSTID phenomenology and causal relation to the presence of SAPS is new and has not been reported before.

Our study also addresses a less explored research area involving TID propagation in the polar region. It is generally thought that auroral generated AGWs/TIDs propagate away from the disturbance source latitudes, moving equatorward into lower latitudes and poleward into higher latitudes. In the polar region, there have indeed been reports of trans–polar cap propagation of TIDs/AGWs from the nightside into the dayside (Balthazor & Moffett, 1999; Cai et al., 2011; Fedorenko et al., 2015; Johnson et al., 1995). In this study, however, we demonstrate an event characterized by predominant trans-polar propagation from the dayside into the nightside, opposite to the expected propagation direction for a disturbance source located in the nightside aurora. These new findings raise important questions regarding storm time TID/AGW source and excitation processes at high latitudes. Our results emphasize a community need in TID propagation studies to clarify and quantify the potential conditioning influence of, and interplay with, background antisunward plasma convection conditions across the polar cap.

2. Solar Geophysical Conditions and Observational Data

Strong geospace disturbances occurred following the arrival of a Coronal Mass Ejection (CME) and a subsequent high speed stream during 7–8 September 2017. A clear interplanetary magnetic field (IMF) Bz southward turning occurred at ~21 UT on 7 September and reached a minimum of −22 nT near 00 UT on 8 September, when the solar wind speed suddenly elevated. A second significant Bz southward turning took place at ~12 UT on 8 September 2017. This later event was associated with a substorm onset during which the AE index reached >2,500 nT. By was modestly negative at 02–03 and 09–11 UT on 8 September. See Figure 1 for variations of solar geophysical parameters including Bz, By, solar wind speed, AE index, Dst index, and Kp index. This time period saw also several solar flares including a X1.3 event peaking at ~14:36 UT on 7 September along with other M-class events. The X9.3 flare on 6 September was previously found to be associated with postflare TIDs near the solar terminator (Zhang et al., 2019). Results of that study also indicated the X9.3 and X1.3 flare events were associated with synchronized ionospheric oscillations over the entire CONUS. Super large structures of plasma density depletion were also identified over Asia and America sectors during two periods of southward Bz (Aa et al., 2018a, 2018b).

This TID study utilizes GNSS TEC observational data generated at MIT Haystack Observatory (Rideout & Coster, 2006; Vierinen et al., 2016) and archived in the Madrigal database (http://www.openmadrigal.org). TID analysis is based on differential TEC processing as described in Coster et al. (2017) and Zhang et al. (2019, 2017) along with extensive discussion regarding the detrending method and the use of different sliding window lengths. Here we provide a short summary.

Differential TEC are determined based on original data from individual pairs consisting of a GNSS receiver channel and a GNSS satellite. These original data have a nominal 15-s resolution with linear interpolation or resampling applied to intervals where original data was not uniformly available. A 30° cutoff elevation for ground-satellite raypaths is used to eliminate data close to the horizon. Calculation of background TEC variation, forming the basis of detrending operations, was obtained using a low-pass Savitzky-Golay filter (Savitzky & Golay, 1964). The algorithm used a convolution process with least squares fitting of successive subsets of windows of a given length (e.g., 30 or 60 min). Fitting used time-adjacent TEC data points from the

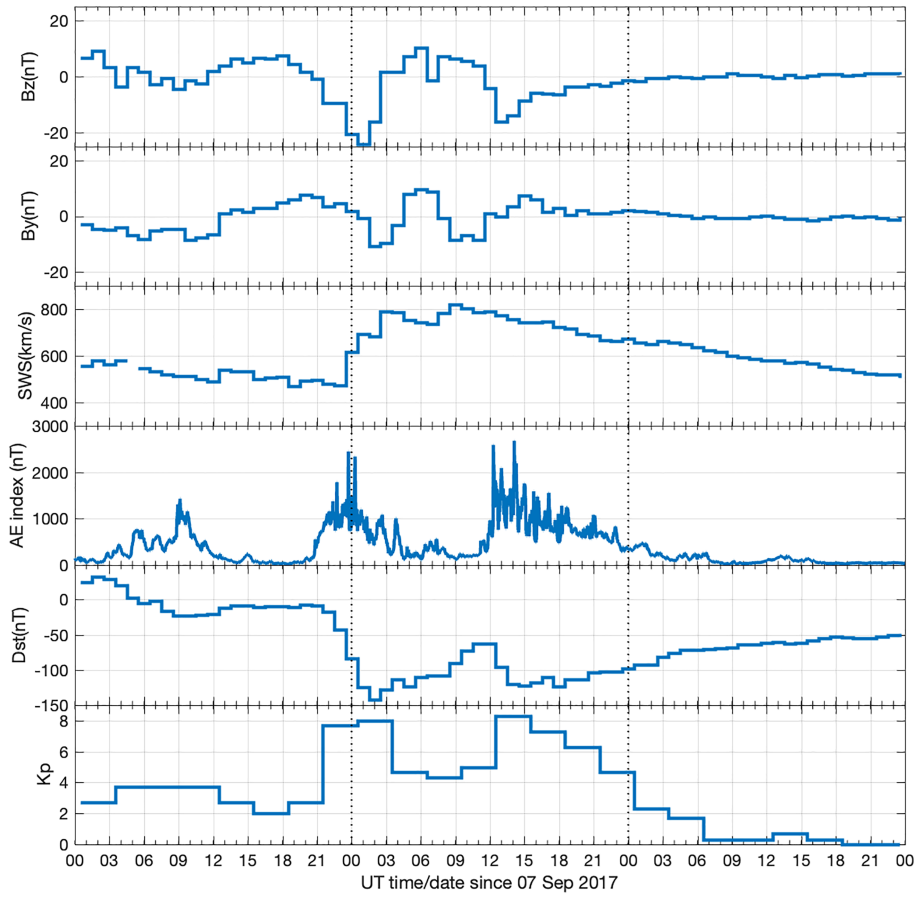

Figure 1. Solar wind and magnetic activity indices during the period of 7–9 September 2017, including interplanetary magnetic field Bz and Bx, solar wind speed, AE index, Dst index, and Ap index.

same GNSS satellite-receiver pair combined with a linear basis function set. Detrended data were analyzed only for time ranges free of "edge effects;" that is, data were included between $t_1 + w/2$ and $t_2 - w/2$ where t_1 and t_2 are the start and end times of the data segment for a given pair of satellite and receiver, and w is the length of the sliding window in time. Small data portions affected by detrending assumptions at the edges of the data were discarded.

To maintain an effective focus on waves with periods ≤30 min relevant to both LSTIDs and MSTIDs, a 30-min sliding window was used in this study. Therefore, background TEC trend results contained perturbation periods longer than 30 min, and after detrending, residual perturbations in differential TEC contained periods shorter than 30-min, and also reduced amplitudes for longer (>30 min) periods. Effectively, the use of a 30-min sliding window method formed a targeted bandpass filter for the class of TID waves to be investigated. We note that such a filter is appropriate primarily for enhanced observations of MSTIDs, whereas by contrast the LSTID results from differential TEC should be fundamentally similar to those derived from using a longer (e.g., 60-min) sliding window method.

This study also utilizes zonal ion drift data in the F region as derived from incoherent scatter radar (ISR) observations at Millstone Hill (42.6°N, 288.5°E). In order to measure the zonal ion drift, the radar made line-of-sight measurements (S_1 and S_2) with −40.5° and −12.0° azimuth in the magnetic meridian, all at 45° elevation. Therefore, assuming the directional cosine for the magnetic southward direction does not change significantly between the two azimuth directions, the westward ion velocity $\mathrm{VperW} = (S_1 - S_2)/\mathrm{cosY}_1$, where $\mathrm{cosY}_1 = -0.32$ (for ~300 km) is the directional cosine for the magnetic eastward direction at −40.5° azimuth. The mean line-of-sight measurement errors for these azimuth directions at 45° elevation were on the order of 30 m/s in the F region; assuming rough quadrature, the derived VperW therefore would have a measurement error of ~50 m/s.

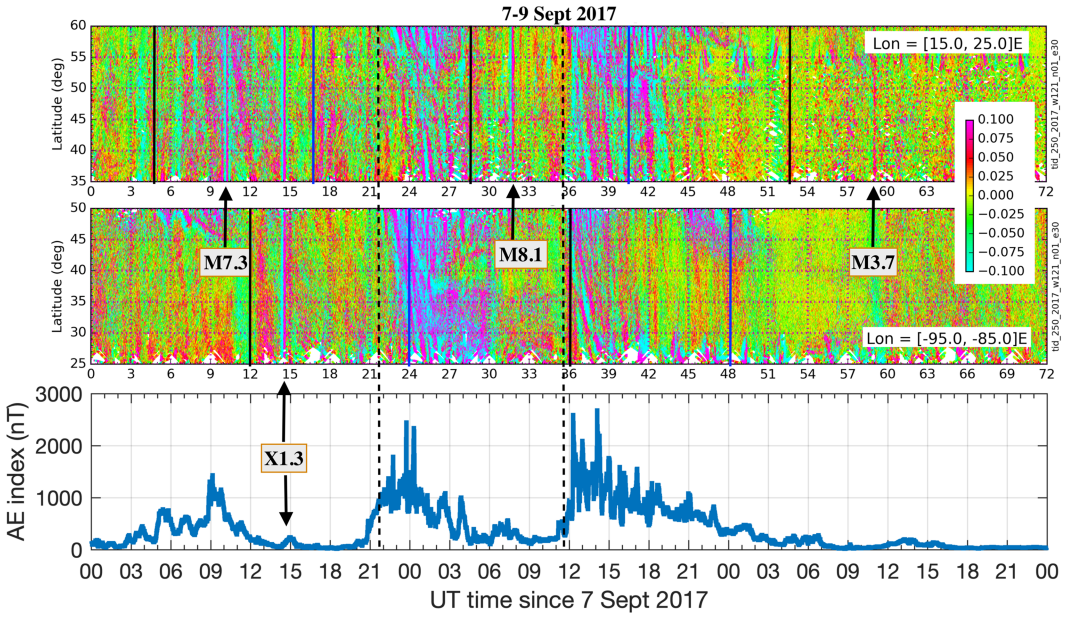

Figure 2. An overview of TID equatorward propagation during the 3-day time period 7–9 September 2017 in the European sector (15–25°E; top) and the American sector (−95–085°E; middle), and their correlation to the AE index (bottom). Solar flare timing is also marked for M7.3, X1.3 M8.1, and M3.7 events visible in these longitudes during the period. The sunrise and sunset terminators are also marked as black and blue vertical lines, respectively.

3. Results and Discussions

With the arrival of the interplanetary disturbances at Earth, IMF Bz turned southward around 2100 UT on 7 September, which immediately produced AE enhancements and launched a variety of TIDs at high latitude, which propagated into lower latitudes. In this section, we discuss TID occurrence timing, spatial pattern of the wave fronts, and propagation characteristics.

3.1. TID Occurrence Timing

After storm onset, TIDs first occurred in less than 1 hr after Bz southward turning at high latitudes and appeared almost simultaneously over CONUS and European sectors. Both sectors were primarily at night. A set of strong and organized TIDs subsequently propagated equatorward. As shown in Figure 2, these strong TIDs remained active for a total of ~6+ hr, when AE was above 1,000 nT after ~22 UT on 7 September. A second set of major disturbances were launched concurrently with a sharp increase of AE between 12 and 13:00 UT on 8 September. The second class of TIDs occurred by contrast within at dayside sectors, with an intensity level nearly equal to the earlier nighttime sector TIDs but with a longer survival time >6 hr in European sector as compared to CONUS. During the same three day period between 7 and 9 September, the four brightest solar flare (M7.3, X1.3, M8.1, and M3.7 classes) occurred when the planet was rotated such that flare impact was visible to the entire sunlit ionosphere over the European and CONUS sectors. This solar disturbance input generated TEC enhancements readily detected with this very sensitive differential TEC technique, and furthermore, the enhancements have features allowing them to be easily distinguished from those propagating TIDs.

3.2. TID Spatial Patterns

We now examine the observed storm time TID spatial patterns, which yield clues about likely TID source locations. Figure 3 present four TID examples with a global view, focusing mostly in the northern hemisphere and corresponding to different IMF/AE index conditions. As the CME arrived after ~21:00 UT, well-organized large-scale wave fronts occurred initially at ~23:00 UT, aligned along approximately zonal circles of constant apex latitude. Subsequently at ~23:00 UT, more complex TID patterns became very evident. Figure 3a shows *concurrent* MSTIDs and large spatial scale TIDs (LSSTIDs) (Type I) beginning at 23:10 UT when the CONUS was in afternoon and dusk sectors. The small wave fronts were aligned in the NW-SE direction and remained propagating westward, rotated, and evolved in amplitude for the next hour or so. (Further discussions about these concurrent TIDs will be given in the next section.)

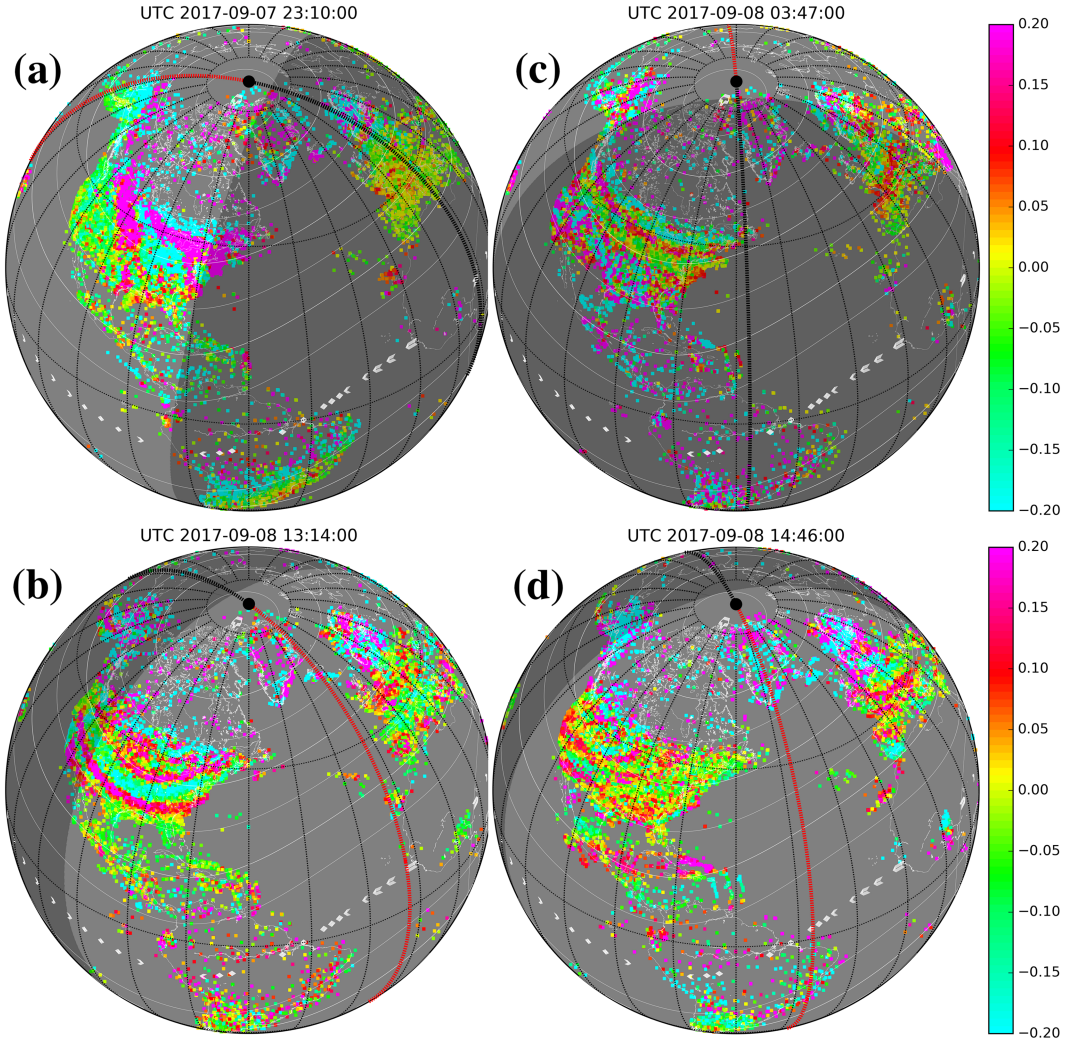

Figure 3. Characteristic pattern types of TID spatial structures observed during 7–8 September 2017 storms. Type I near dusk shown in (a), and Type II near dawn shown in (b), are concurrent large and medium-scale TIDs, where medium-scale TIDs in Type I are aligned NW-SE and in Type II NE-SW. Type III shown in (c) appeared as super large scale TID wave fronts across continents. Type IV shown in (d) constituted regional TIDs. White thin lines mark the iso-apex latitude at a 10° interval.

Figure 3b shows a second type of wave front (Type II) occurring at 13:14 UT and represent concurrent MSTIDs and LSSTIDs at 13:14 UT when the CONUS was in the dawn and morning sector. As discussed in the next section, a strong eastward propagation of TIDs, opposite to the first type just described, occurred during this time period as secondary MSTID wave fronts emerged. These latter MSTID fronts, however, were aligned in the NE-SW direction and were located at middle to subauroral latitudes, lagging behind the main LSSTID fronts at midlatitudes. These concurrent TIDs are distinct from the first type of concurrent TIDs mentioned earlier, in which secondary MSTID fronts, accompanied by westward propagation and rotation of TIDs, were ahead of the main LSSTID wave fronts.

A third type of TID wave fronts (Type III) occurred at 03:47 UT, with very large zonal scales (Figure 3c) spanning at least 50° in longitude at ~55°N apex latitude, or ~4,000 km, from the U.S. West Coast to the East Coast. Simultaneous wave fronts were also observed at this time in Alaska (afternoon sector), and in Europe (dawn and morning sectors). Multiple wave fronts organized in the zonal direction were also seen at Europe, CONUS, and Alaska sectors.

Finally, a fourth type of wave fronts (Type IV) appears to be regional specific structures although all driven by enhanced magnetic disturbances (Figure 3d). These multiple fronts occur simultaneously in both Europe

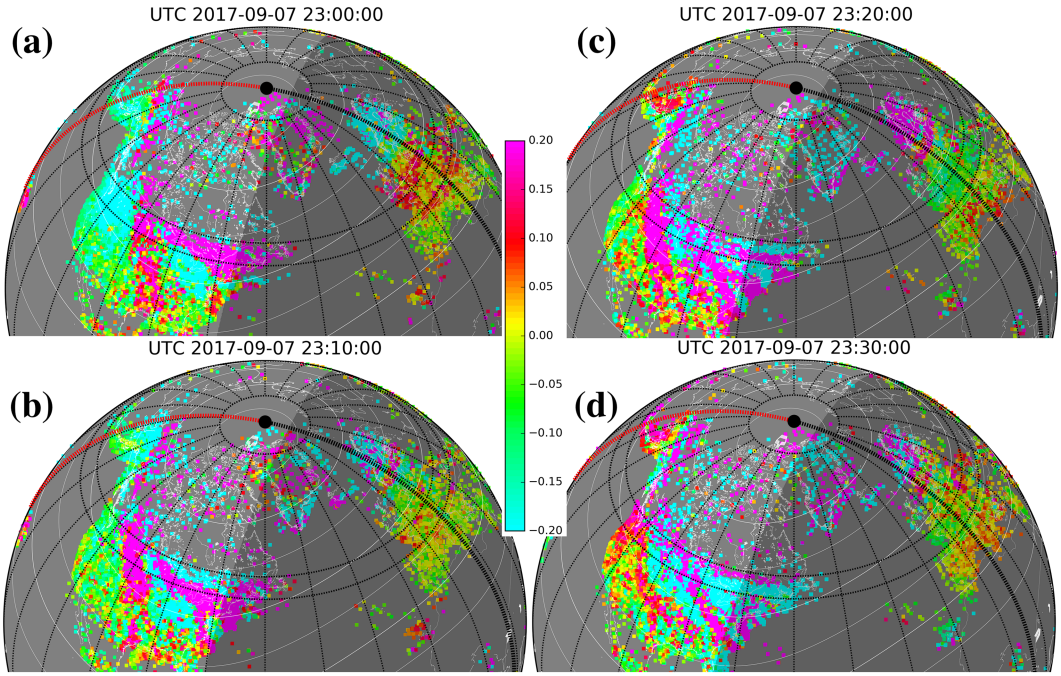

Figure 4. A sequence of TID maps between 2300 and 2330 UT on 7 September demonstrates dynamic evolution of concurrent large- and medium-scale TIDs near the dusk sector as a bright SAPS feature occurred. White thin lines mark the iso-apex latitude at a 10° interval. The double black circles mark the 45–50°N latitude range which is the cross section used for the keogram in Figure 5.

and CONUS sectors but they are regional ring-shaped waves suggesting localized excitation sources. For example, the CONUS disturbance source appears at high latitudes near the dawn sector while the European disturbance source appears at high latitudes but near the dusk sector.

3.3. Concurrent MSTIDs and LSSTIDs

In the following discussion, we focus on the unusual storm time appearance of concurrent MSTIDs and LSSTIDs near subauroral latitudes and explore their correlation with subauroral dynamics.

After creation, LSSTIDs propagated away from their high-latitude source into subauroral latitudes (Figure 2). In these regions, a westward propagation component became increasingly evident and strong (Section 3.2), and eventually one of the large wave fronts appeared breaking and a new secondary smaller wave fronts at midlatitudes emerged. An animated movie as a supplement to this paper demonstrates the development of various wave activities at 1 min cadence between 22 and 01 UT during 7–8 September. Figure 4 shows these quickly evolving processes at a 20-min cadence. Details of the midlatitude westward wave propagation component are contained in the keogram for 45–50°N; see Figure 5a. Once onset of TIDs at these latitudes occurred at ~21:00 UT, they propagated westward approximately along the sunset terminator (dashed line) at a zonal phase speed of ~320 m/s (arrow marked as (2)). However, the westward component of propagation increased immediately to ~720 m/s (arrows marked as (3)).

At ~23:00 UT during American sector intensification of westward TID amplitudes, a simultaneous TID wave front in the zonal direction was launched in Europe (0–50°E) with very significant amplitude (the left most double-headed arrow marked as (1) in Figure 5). Subsequent arrivals of similar wave fronts (aligned in the zonal direction) in Europe were clearly observed at ~45- and ~60-min delays (the two right-side double-headed arrows marked as (1) in the figure). Eastward propagation occurred later postmidnight. By contrast, the European sector (0–50°E), at lower magnetic latitudes than the American sector (−130°E to −50°E), had wave activity characterized more properly as midlatitude midnight structures (marked as (1)).

The enhanced westward wave propagation in the American sector, and simultaneous zonal wave fronts in Europe, occurred when huge zonal ion drifts were observed. Millstone Hill ISR observations captured these zonal ion velocities, and Figure 5b indicates peak zonal ion drifts in the *F* region for 2.0 km/s. These magnetic latitude aligned velocities, with latitudinal width of a few degrees, formed a clear signature of a

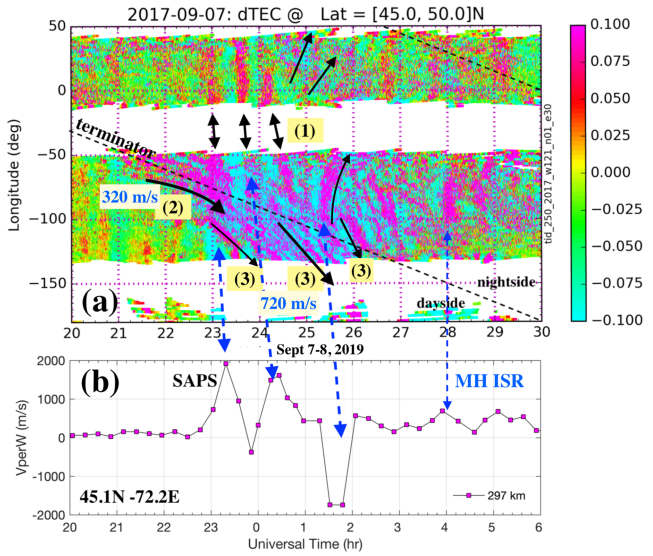

Figure 5. Zonal propagation of TIDs at 45–50°N latitudes near the dusk sector from GNSS TEC observations (a) and the associated F region westward ion velocity measured by Millstone Hill ISR during 20–06 UT on 7–8 September 2017 (b). Double-headed arrows (1) represent TID zonal wave-fronts in the European sector; Arrow (2) identifies TIDs propagating westward along the terminator direction at 320-m/s phase speed; Arrows (3) identify westward TIDs with enhanced propagation speed at 720 m/s following the launch of strong zonal ion drifts (including SAPS).

strong SAPS (Foster & Burke, 2002). A secondary westward drift subsequently moved into the radar's field of view slightly after 00 UT on 8 September. A large storm enhanced density (SED) plume (Foster et al., 2002) was also observed during this time frame but emerged prior to the SAPS launch at Millstone Hill latitudes, with SED plume and Tongue of Ionization (TOI) structures persisting for a few hours (Figure 6). TOI shown in the figure was observed off the magnetic pole, more close to the dusk cell when the IMF By became negative. A strong upward ion drift (up to 100 m/s at 450 km and larger at higher altitudes, figure not shown) was also observed at 23:18 UT, likely caused by penetrating electric fields as IMF Bz became strongly southward. These results suggest that SAPS-related strong westward ion drift might have induced the enhancement of LSSTID westward propagation components and may have even excited MSTIDs. It is important to note that while the westward SAPS was ~2,000'm/s, the associated TIDs under discussion had a zonal (westward) speed of less than half of that, within the typical LSTID range.

The presence of SAPS channels during the September event provided several potential impacts relevant to TID dynamics. Studies have found that SAPS can directly accelerate the background zonal wind via strong ion drag (e.g., Ferdousi et al., 2019; Wang et al., 2011; Zhang et al., 2015) and can indirectly change the meridional wind through the Coriolis force (Zhang et al., 2015). SAPS can cause strong frictional heating (e.g., Zhang et al., 2017) to both neutrals and ions and therefore can change the neutral density and composition in nearby regions (Guo et al., 2018; Wang et al., 2012). Neutral atmospheric changes in these various parameters will alter the AGW propagation conditions, thus modifying GWs and LSSTIDs as they propagate through subauroral latitudes. Additionally, the appearance of SED plumes with highly elevated plasma density near the SAPS region can provide extra damping to the passing AGWs/LSSTIDs. Furthermore, these plumes are spatially inhomogeneous structures (see Figure 6) with changing alignment during the course of their convection and evolution, leading to different damping forces on different segments of the same wave front. Finally, it might be also possible that SAPS flows initiated new AGWs and TIDs with a westward propagation component. Simulations by Guo et al. (2018) have suggested that SAPS related thermospheric heating can possibly induce regional thermospheric and ionospheric disturbances taking the form of TIDs/AGWs as anticipated in Zhang et al. (2017).

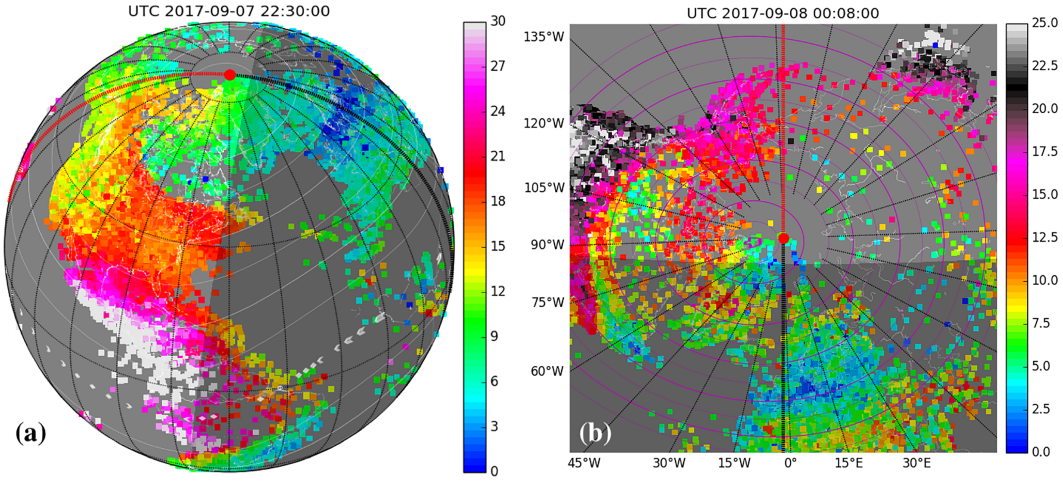

Figure 6. TEC structures at subauroral latitudes with SED plume (a) and high latitude with TOI (b) during the time period of strong dynamics at subauroral latitudes between 22:30 UT on 7 September and 00:08 UT on 8 September. White circles are apex latitudes between 40° and 90° at 10° interval.

Several possibilities exist for MSTID generation during this event. The PI (Fukao et al., 1991; Makela & Otsuka, 2011; Perkins, 1973; Saito et al., 2001) is well known as a potential modulating process for multiple aspects of midlatitude dynamics during both quiet and disturbed conditions. This raises the interesting possibility that PI associated physics might provide a means for storm time excitation of MSTIDs, in a similar fashion as observed at midlatitudes during nighttime conditions. In fact, the MSTID wave fronts reported here are aligned in the northwest to southeast (NW-SE) direction, characteristic of the preferred Perkins direction and similar to typical nighttime MSTIDs at midlatitudes. Thus, upward ion drift can be produced by the polarization electric field, established when the Pedersen current flows across the MSTID wave front in NW-SE and can support sustained PI growth rates. For these reasons, one possible suggested scenario for the conditions studied here might involve a LSSTID wave front passage through subauroral latitudes, encountering the SAPS flow channel with strong westward ion drifts. They modified the TAD (AGW) associated with the LSSTID due to changing thermospheric winds (Ferdousi et al., 2019; Wang et al., 2011; Zhang et al., 2015), composition and temperature conditions (Guo et al., 2018; Wang et al., 2012) as a result of SAPS induced ion-neutral coupling. These changes, in particular, in neutral temperature and winds could be altitude dependent and highly regional to the SAPS channel and would affect the AGW wave propagation mode. Eventually, they would drive the TAD (AGW)/LSSTID wave fronts to rotate westward. This NW-SE bend of electron density homogeneity would then allow the development of a polarization electric field with an eastward component due to the Pedersen current driven by the poleward SAPS electric field, thus providing growth for the PI and MSTID generation. A large simultaneous penetrating electric field producing a strong vertical ion drift may also contribute to the instability growth. This is because the maximum PI growth rate is inversely proportional to the ion-neutral collision frequency and the scale height (Perkins, 1973). As the penetrating or polarization electric field moves plasma upward to higher altitudes, the ion-neutral collision frequency reduces dramatically due to its exponential function dependence on height. Another alternative MSTID excitation process could come from local ion and neutral heating, as mentioned earlier, due to the presence of a strong SAPS electric field (Guo et al., 2018). Further investigation, especially simulation work, is needed to provide detailed physical insights and quantitative estimations of competing processes involved in order to establish the most likely physical process link between SAPS and MSTIDs.

Regarding westward motion of disturbances, westward propagation and the increase of zonal propagation velocity occurred not just at subauroral latitudes but also at lower latitudes (at least to 25°N, figure not shown) in the American sector. This suggests also that penetration/expansion of magnetospheric (ionospheric high latitude) convection near dusk with strong westward components may have developed around 00UT on 8 September and may responsible for the enhanced TID westward propagation.

A different MSTID eastward propagation scenario near the morning sector is possible and appears to be correlated with the eastward return flow of the plasma convection, in sharp contrast with the earlier MSTID scenario characterized by westward propagation near dusk during the presence of SAPS. Specifically, significant TID zonal propagation was observed in the dawn sector during 12:00–15:00 UT when the IMF Bz was persistently southward; see Figure 7. TIDs can be easily identified during this time with a 800 m/s eastward phase speed, and corresponding zonal ion drifts measured by the Millstone Hill ISR were eastward, up to 600 m/s. This appears to be part of the morning eastward convection cell which is typically within auroral latitudes, but this cell was likely expanded to Millstone Hill latitudes for this case. The MSTIDs shown in Figure 3c for 13:14 UT occurred during this time frame. Similar MSTID examples are also given in Figures 8a and 8c for 12:38 and 13:22 UT, respectively. These MSTIDs propagated in the same direction as expanded eastward convection at comparable velocities, with wave fronts primarily in the NE-SW direction but rotated into the zonal direction. Thus, we suggest that eastward convection is likely playing a role in the MSTID structuring.

Shiokawa et al. (2012) previously reported a nighttime MSTID event at the high-latitude location of Tromsø, Norway (magnetic latitude: 67.1°N). The study found that MSTIDs propagated eastward and began oscillating at the time of auroral brightening. They suggested that MSTIDs, initially created along with AGWs, were left as fossil plasma structures that evolved under the influences of auroral convection electric fields. Our MSTID observations show similar influences of the convection electric field; however, in the study presented here, the initial excitation of MSTIDs was presumably associated with conventional auroral heating. The instability mechanism mentioned earlier near the dusk sector provides another potential candidate for wave excitation. Nishi et al. (2018) and Shiokawa et al. (2014) reported finger-like auroral brightness structures at

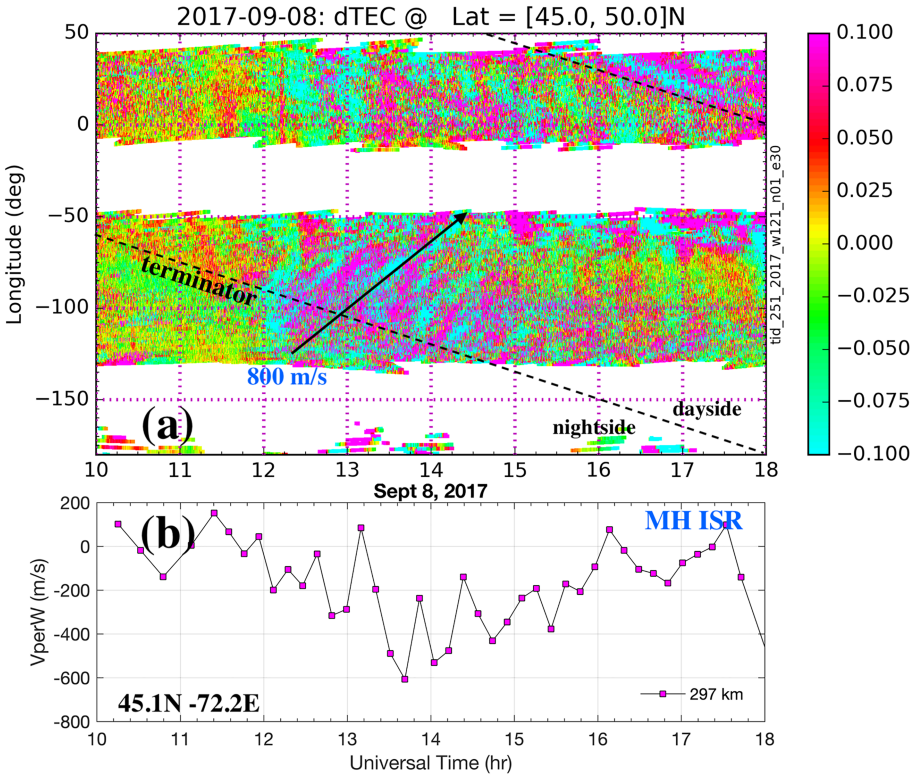

Figure 7. Zonal propagation of TIDs at 45–50°N latitudes near the dawn sector from GNSS TEC observations (a) and associated *F* region westward ion velocity measured by Millstone Hill ISR during 10–18 UT on 8 September 2017. The eastward propagation of TIDs occurred at 800 m/s, larger than the eastward ion drift measured by the Millstone Hill ISR.

postmidnight sectors near the equatorial boundary of an auroral arc. These brightness structures were organized latitudinally with horizontal-scale sizes ranging from 15–100 km, moved eastward with slow speeds of 150–400 m/s, and were considered as auroral fragmentation into patches. Multiple electron density structures, shown as differential TEC fluctuations in Figures 8a and 8c, seem qualitatively different from those auroral patches, as TEC structures were clearly eastward aligned with definite spatial periodicity and substantially faster motion. The corresponding TEC maps (b) and (d) showed no clear sign of auroral induced TEC enhancements.

TEC (absolute value) enhancements that were elongated northeastward toward higher latitudes and the noon sector as shown in Figure 8c were similar to nominal SED plume structures, which extended toward high latitudes and the noon sector with a base near the dusk, excepting a base near the morning sector. In this case, the eastward convection may have convected the morning sector plasma sunward into higher latitudes and noon sectors.

3.4. Global Propagation

Discussions so far have focused primarily on midauroral and subauroral latitude TIDs as an important part of the global TID picture. Figure 9 further shows a picture of meridional propagating TIDs at CONUS longitudes ~ −70°E (bottom portion) and European longitudes ~15°E (upper portion). These longitude sectors have a 6-hr offset (see the vertical dashed line for approximate day-night terminators), with magnetic latitudes having a more than 10° offset. In the keogram of Figure 9, the arrows trace observed phase propagation directions of TIDs, and the slope of the arrows represents the TID propagation speed.

In the ~ −70°E CONUS sector, we found that nighttime equatorward TIDs, associated with high-latitude heating following the CME arrival and Bz southward turning around ~21:00 UT, were evident and well organized in both hemispheres as shown by Arrows (1) and (2). These TIDs penetrated deep into the equatorial region. TID amplitudes in the Northern Hemisphere remained larger, although throughout the night, the Southern Hemispheric TIDs remained active (e.g., Arrow (3)).

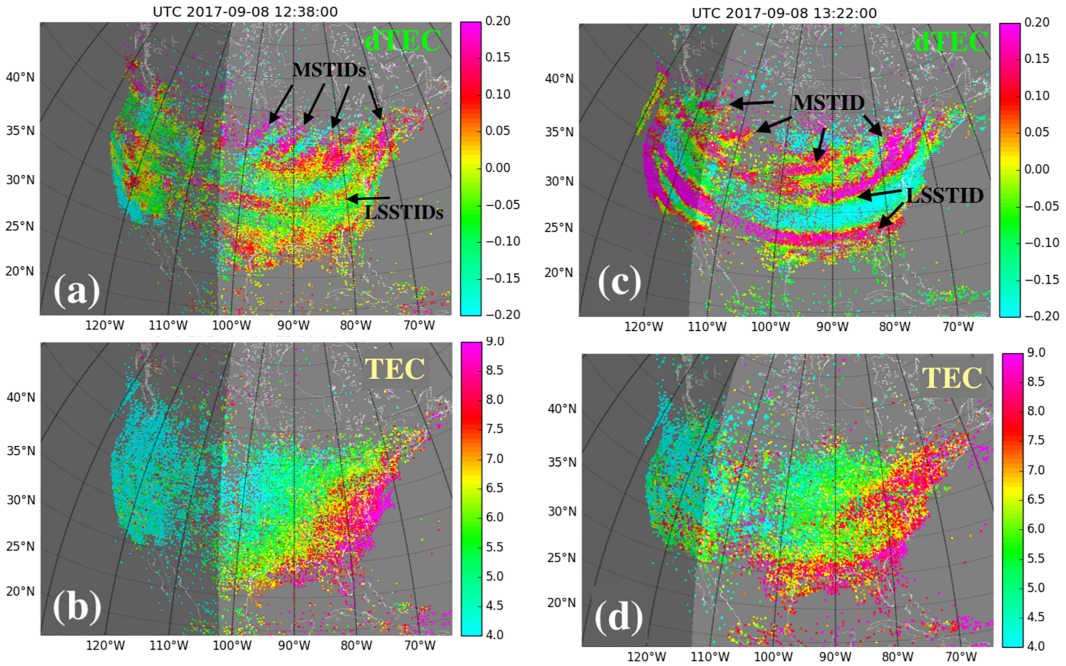

Figure 8. Concurrent MSTIDs and LSSTIDs near the dawn sector at 12:38 UT (a) and 13:22 UT (c) as well as their corresponding TEC at 12:38 UT (b) and at 13:22 UT (d) on 8 September.

Figure 9 also indicates that the TID activity became stronger with the second Bz southward turning at 12:00 UT on 8 September. The ~ −70°E CONUS sector was on the dayside at the time. Strong equatorward propagating TIDs occurred for both hemispheres starting from ~13:00 UT (Arrows (4)–(6)). These TIDs had very large zonal wave fronts as shown earlier in Figure 3. We therefore conclude that cross-equator propagation existed (Arrows (4) and (5)); similar cross-equator propagation TIDs were previously reported. It is interesting to note the slopes of these TIDs. These slopes are consistent with a meridional phase speed ~550 m/s

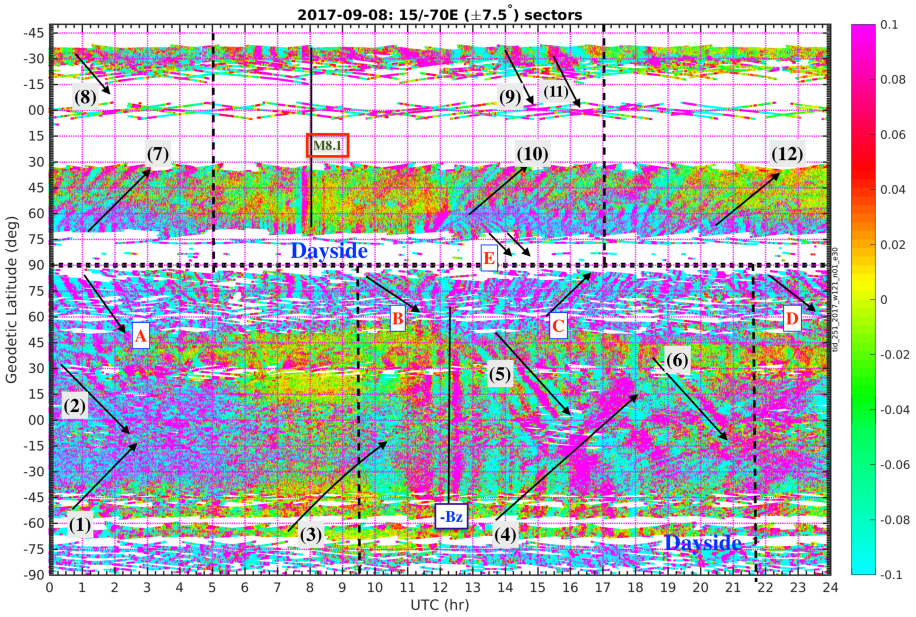

Figure 9. Keograms of differential TEC showing meridional propagation of TIDs for eastern America sectors (−70°E, bottom) and European sectors (15°N, top). TID propagation directions at middle and low latitude are marked by Arrows (1)–(4) in the America sector and (7)-(12) in the European sector. TID propagation directions in the northern polar region are marked by Arrows (A)–(E). M8.1 solar flare is also marked, as well as the time when Bz turned to southward. Vertical dashed lines are terminators.

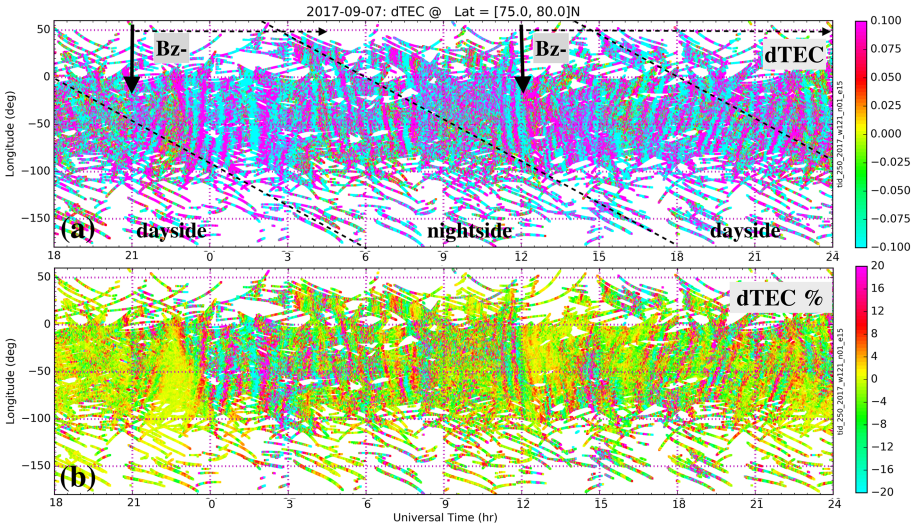

Figure 10. Keogram showing the disturbance zonal propagation in differential TEC (a) and the percentage differential TEC relative to the background (b) at the latitude range 75–80°N during 7–8 September 2017. The vertical phase fronts indicate the zonal scale size of the disturbances, which typically spans 100+° longitudes, equivalent to 2,000+ km at 80°N. The zonal propagation is predominately westward in the morning sector (near the central diagonal dashed line), and eastward in the afternoon sector, both with an anti-sunward component in the polar cap.

for the Southern Hemisphere and ~670 m/s for the Northern Hemisphere. Both are typical LSTID speeds (with <30-min periods), but the TIDs in the Northern Hemisphere were faster than in the southern hemisphere. These dayside TID speeds appear to be very comparable with the nightside ones perhaps due to the disturbance source intensities (as indicated by the AE index) being similar, although damping effects during daytime forcing, manifesting as TID propagation attenuation, was potentially larger due to higher plasma density. On the other hand, the dayside TID amplitudes appeared to increase as the TIDs traveled into the low and equatorial latitudes where the background plasma density increased dramatically as magnetic field lines became increasingly horizontal. Therefore, for the same source disturbance, the TID amplitude could depend significantly on both the background plasma density and magnetic inclination (Tsugawa et al., 2004).

As shown in Figure 9, in the ~15°E European sector, equatorward TIDs in both hemispheres were evident for both the nightside (Arrows (7), (8), and (12)) and the dayside (Arrows (9)–(11)). The meridional phase speeds were also comparable for both the dayside and nightside but appeared to be slower than corresponding ones in the CONUS sector by ~100 m/s, perhaps due to lower magnetic latitudes with correspondingly longer distances from the magnetic high-latitude source region.

3.5. High Latitudes

Of particular interest to this study is high-latitude TIDs and their propagation. The convectional expectation is that nighttime auroral zones form the main source of TID excitation and TIDs should propagate away from the source region: equatorward into lower latitudes and poleward into the polar region. However, for the study event, Figure 9 does not seem to provide evidence consistent with this general scenario. In the CONUS sector, the nightside TIDs from polar cap to auroral zones (the Arrows A and D) are clearly equatorward, consistent with the subauroral and midlatitude TID propagation as if the disturbances propagated from the magnetic pole all the way into middle and low latitudes. Arrow B in the morning sector at high and polar latitudes points to equatorward TIDs. Dayside TIDs (around midday as indicated by the Arrow C) are, however, clearly poleward of these regions. Similar dayside poleward TIDs may have existed in the European sector at very high latitudes (the Arrow E) but could not be observed due to GNSS orbital geometries. Thus, poleward propagation in the polar cap and equatorward propagation at subauroral and midlatitudes (Arrows (5) and (6)) seem to be consistent with the assumption that TIDs were excited in the dayside high latitudes (auroral or cusp latitudes).

In general, polar region TID propagation during the study event can be summarized as being strongly poleward on the dayside, strongly equatorward on nightside, and weakly equatorward on the morning side. This pattern appears analogous to the antisunward plasma convection flow across the polar cap, as part of the well-known two-cell convection at high latitudes. However, it should be emphasized that these TIDs

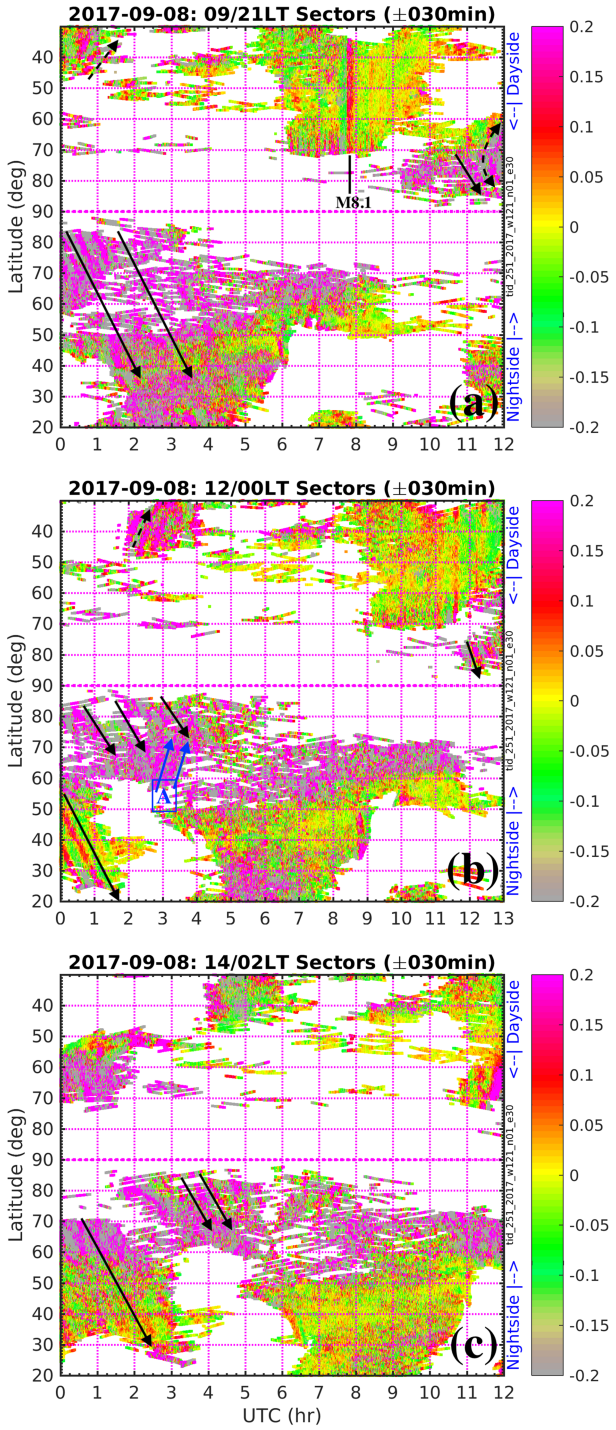

Figure 11. Keograms of differential TEC as a function of latitude and UT for local time sector pairs in each panel during the period of first IMF Bz southward period: (a) 09 LT (top)/21 LT (bottom); (b) 12 LT (top)/00 LT (bottom); and (c) 14 LT (top)/02 LT (bottom). In each panel, the dayside sector is on the top and the nightside sector is on the bottom. Black solid arrows indicate that the transpolar propagation is dayside-to-night. See text for further discussion.

are truly TIDs and not artifacts of the convection flow carried by, for example, the tongue of ionization TOI or polar patches, as supported by the following arguments: (1) The trans-polar TID phase speed was 500–600 m/s, within the typical large-scale AGW propagation range. This is significantly slower than the convection flow for nominal geomagnetic activity, which is intensified during a sustained Bz southward period. (2) The scale size of zonal wave fronts was persistently much larger than that of plasma structures such as polar patches. (See Figure 10a for a keogram of the disturbance wave fronts and zonal propagations at 75–80° latitudes.) The wave fronts of these zonal structures formed almost continuous vertical lines in the keogram and were very well organized periodically, suggesting significant spatial coherence of the structures. These structures were persistent and clearly spanned a very large spatial region of 100+° longitudes at 75–80°N latitudes, or 2000+ km in the zonal direction. Furthermore, these structures were much larger than the typical size of polar patches (Zhang et al., 2013), which are ~500 km or smaller (Coley and Heelis (1995) used 100–1,000 km to classify patches.) The zonal propagation of disturbances shown in Figure 10 is also very clear: being westward in the morning sector (with an anti-sunward component in the polar cap) and eastward in the afternoon sector (also with an anti-sunward component in the polar cap). (3) The amplitude of these structures, derived from the 30-min sliding window detrending method, was normally 15% or less (see Figure 10b showing percentage amplitudes of the differential TEC). Note that this value might increase to 30% or less if a 60-min sliding window de-trending method is utilized (not shown here). Nevertheless, these amplitudes remain substantially smaller than typical patch amplitudes around 200% (Ren et al., 2018).

To further demonstrate transpolar day-to-night meridional propagation of TIDs at high latitudes, we provide a few sets of keograms organized by pairs of local times (rather than longitudes in Figure 9). These pairs consist of dayside and nightside parts of the north polar region. Figure 11 shows TIDs associated with the first period of Bz southward, with local time pairs of morning-evening 09/21 LT (a), noon-midnight 12/00 LT (b), and postnoon-postmidnight 14/02 LT (c), with the dayside on the top and the nightside on the bottom in each panel. Panels (a)–(c) all indicate the nightside portion of equatorward (approximately morning-to-evening, noon-to-midnight, and postnoon-to-postmidnight) propagation (see black arrows at high latitudes). Figure 12 shows TIDs associated with the second period of Bz southward (on 8 September), for local time pairs of morning-dusk 07/18 LT (a), noon-midnight 12/00 LT (b), and afternoon-dawn 16/04 LT (c). Panel (a) shows the dusk portion of equatorward propagation (see black arrows at high latitudes); panel (b) shows the noontime portion of the antisunward/poleward propagation (see black arrows at high latitude). We note though that a wave front "reflection" and directional reversal may potentially be seen in panles (c) and (a) (bent dashed line arrows) corresponding to the morning sector near 65°N (CONUS sector) and afternoon sector TIDs near 70° (European sector), respectively. This wave front directional change occurred in Figure 11a as well (the bent dashed arrow). The location of all these directional changes, probably suggesting the TID source region, was on the dayside (including morning side).

These observations seem to support a speculation that transpolar TIDs were excited on the dayside at those high-latitude locations where TID directional reversal was found. It seems reasonable to ascribe the TID

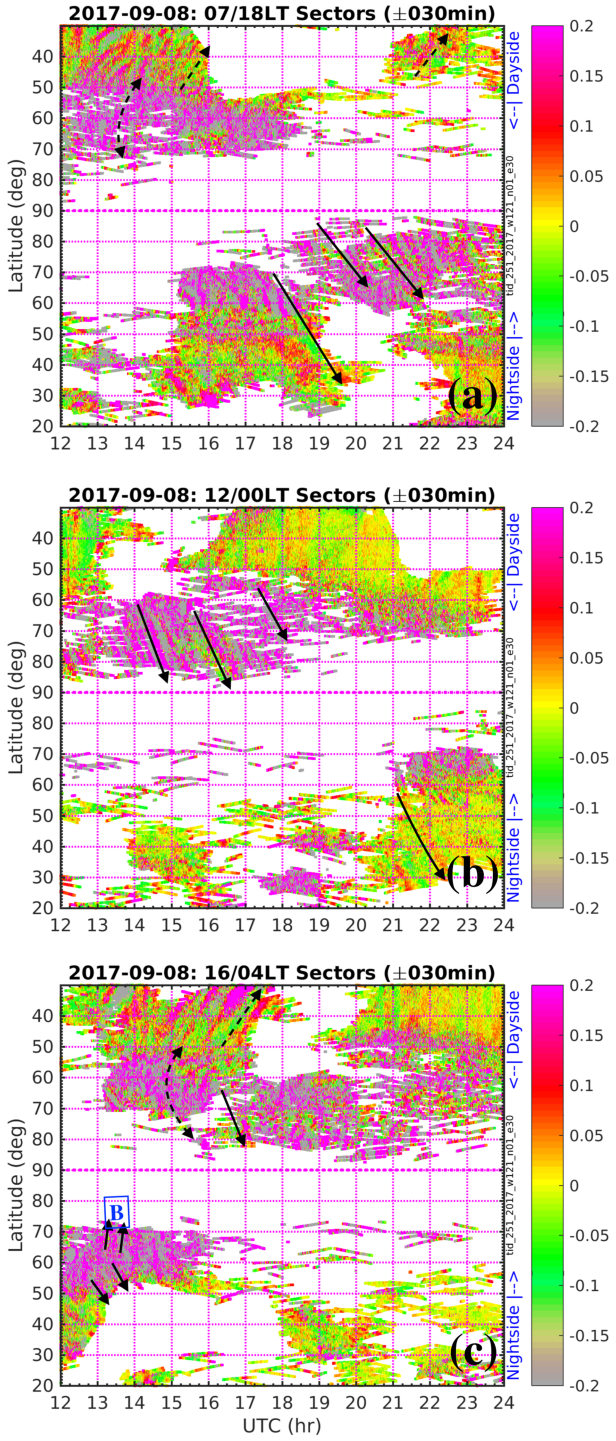

Figure 12. Same as Figure 11 but for the second period of IMF BZ southward and different local time pairs for each panel: (a) 07 LT (top)/18 LT (bottom); (b) 12 LT (top)/00 LT (bottom); and (c) 16 LT (top)/04 LT (bottom).

excitation to the cusp region heating processes during the storm, and storm time cusp or high-latitude heating could have been more efficient in exciting poleward TIDs than the substorm related auroral heating during this 8 September 2017 event. Huang et al. (2017) and Lühr et al. (2004) previously described the frequent occurrence of thermospheric high-density structures in the ionospheric cusp region. These structures were generally accompanied by very intense small-scale field-aligned current filaments, which may lead to significant Joule heating to the ionosphere-thermosphere system. Bristow et al. (1994) also ascribed

SuperDARN measured GWs/TIDs at high latitudes to an excitation source near the cusp region. Dayside auroral intensification structures can subsequently move poleward as "poleward moving auroral forms" (PMAF, Nishimura et al., 2014). Our results highlight that community studies are needed for discovery and understanding of the potential connections between transpolar TIDs and high-latitude multiscale dynamical processes.

In these configurations, background neutral winds would be expected to flow primarily antisunward across the polar cap due to substantial antisunward ion drift. This provides the potential of filtering out AGWs that propagate in the same direction with the similar speed as the winds (Cowling et al., 1971, 1987; Yeh et al., 1972). However, Fabry-Perot interferometer (FPI) observations in the polar cap indicated that the thermospheric winds have hardly exceeded 400 m/s (Wu et al., 2017), making it unlikely that these TIDs/AGWS with the 500–600 m/s phase speed could have been substantially filtered out by these winds. Furthermore, if these TIDs/AGWs were created in situ, for example, within the thermosphere and ionospheric *F* region by Joule heating (Deng et al., 2011), then they would not have to travel a long vertical distance while propagating upward to survive the strong wind filtering.

In addition to day-to-night trans-polar TIDs, expected nightside poleward TIDs at high latitudes existed as well; compare the arrows marked by A in Figure 11b and B in Figure 12b. These nigthside TID components, however, were less organized but traveled faster (larger meridional phase speed) than the predominant antisunward TIDs.

4. Summary

This study has focused on a few unusual disturbance time TID features observed in GNSS TEC during the 7–8 September 2017 geospace storms. These storms were characterized with two periods of IMF Bz southward turning and persistence, yielding significant TID structures that propagated globally and regionally. The TIDs exhibited <30-min periodicity with huge wave fronts, well over 1,000 km and sometimes at least 4,000 km in zonal dimension.

LSTIDs and MSTIDs represent different modes of ionospheric waves and are excited through different physical processes. They are often observed and studied separately. This study challenges that analysis strategy by providing clear evidence of concurrent MSTIDs and LSSTIDs at midlatitudes for both dusk and dawn sectors. While LSSTIDs originated from high latitudes due to magnetospheric energy, momentum and material injections on both dayside and nightside, they subsequently propagated into subauroral latitudes where strong electrodynamics took place to shape the regional thermosphere and ionosphere system. This shaping process changed thermosphere-ionosphere conditions and influenced the propagation of LSSTIDs and atmospheric waves associated with them, and it may lead to excitation of new modes of atmospheric waves and ionospheric disturbances.

Of particular interest, the MSTIDs in dusk sectors appeared to be triggered by a 2,000-m/s SAPS westward ion drift, as measured simultaneously with GNSS TEC observations and the Millstone Hill incoherent scatter radar. With SAPS onset, LSSTID wave fronts, which were aligned originally in the zonal direction, rotated westward and propagated westward at a phase speed of less than half of the SAPS speed, and smaller ionization structures formed and developed into predominately westward propagating MSTIDs. This study provides evidence of strong correlation between SAPS and TIDs. Specifically, enhanced frictional heating associated with SAPS type strong ion velocities may be responsible for the excitation of AGWs/TIDs at subauroral latitudes, which then propagated southwestward over CONUS. Another plausible excitation process is related to PI growth rates over the northwest-to-southeast wave front of plasma density disturbances under the influence of SAPS poleward electric field and magnetospheric penetration electric field.

Near the dawn sector where concurrent MSTIDs and LSSTIDs developed at midlatitudes, MSTIDs were aligned northeast-to-southwest with spatial periodicity and propagated eastward at a speed of 800 m/s, similar to the background eastward ion velocity. These structures were similar to some MSTIDs observed in auroral latitudes (Tromsø) but were different from the auroral patch structures near the equatorial boundary of the auroral arc observed previously in the optical imaging.

Unexpected propagation of TIDs in the northern polar region was persistently observed during almost the entire day on 8 September. Transpolar TID propagation at 500–600 m/s was consistently from the dayside to the nightside, or antisunward along the noon-midnight sector, morning to evening, and afternoon to dawn. These structures had a zonal scale size of 2000+ km at 75–80°N latitudes and a 15% amplitude in TEC. These observations suggest that the dayside source of heating (e.g., near the cusp region) was more efficient

in exciting poleward AGWs/TIDs than the nightside source at auroral latitudes during these 7–8 September storms.

Acknowledgments
GPS TEC data products and access through the Madrigal distributed data system are provided to the community (http://www.openmadrigal.org) by the Massachusetts Institute of Technology (MIT) under support from the U.S. National Science Foundation (NSF) Grant AGS-1762141, which also supports ISR observations and analysis at MIT Haystack Observatory. S. R. Z. and P. J. E. acknowledge NASA LWS funding support (NNX15AB83G); S. R. Z. and A. J. C. the DoD Multidisciplinary Research Program of the University Research Initiative (MURI) Project FA9559-16-1-0364; and A. J. C., S. R. Z., and L. P. G. the ONR Grant N00014-17-1-2186. Data for TEC processing are provided from the following organizations: UNAVCO, Scripps Orbit and Permanent Array Center, Institut Geographique National, France, International GNSS Service, The Crustal Dynamics Data Information System (CDDIS), National Geodetic Survey, Instituto Brasileiro de Geografia e Estatística, RAMSAC CORS of Instituto Geográfico Nacional de la República Argentina, Arecibo Observatory, Low-Latitude Ionospheric Sensor Network (LISN), Topcon Positioning Systems, Inc., Canadian High Arctic Ionospheric Network, Centro di Ricerche Sismologiche, Système d'Observation du Niveau des Eaux Littorales (SONEL), RENAG: REseau NAtional GPS permanent, GeoNet—the official source of geological hazard information for New Zealand, GNSS Reference Networks, Finnish Meteorological Institute, and SWEPOS—Sweden. Data used to generate the TIDs are available from https://w3id.org/cedar?experiment&urluscore;list=experiments2/2017/gps/06sep17&file&urluscore;list=los&urluscore;20170906.001.h5 website and https://w3id.org/cedar?experiment&urluscore;list=experiments2/2017/gps/07sep17&file&urluscore;list=los&urluscore;20170907.003.h5 website, and Millstone Hill ISR data are available from https://w3id.org/cedar?experiment&urluscore;list=experiments/2017/mlh/07sep17&file&urluscore;list=mlh170907g.003.hdf5 website and https://w3id.org/cedar?experiment&urluscore;list=experiments/2017/mlh/08sep17&file&urluscore;list=mlh170908g.003.hdf5.

References

Aa, E., Huang, W., Liu, S., Ridley, A., Zou, S., Shi, L., et al. (2018a). Midlatitude plasma bubbles over China and adjacent areas during a magnetic storm on 8 September 2017. *Space Weather*, *16*, 321–331. https://doi.org/10.1002/2017SW001776

Aa, E., Zou, S., Ridley, A., Zhang, S.-R., Coster, A. J., Erickson, P. J., et al. (2018b). Merging of storm-time midlatitude traveling ionospheric disturbances and equatorial plasma bubbles. *Space Weather*, *17*, 285–298. http://doi.org/10.1029/2018SW002101

Balthazor, R. L., & Moffett, R. J. (1999). Morphology of large-scale traveling atmospheric disturbances in the polar thermosphere. *Journal of Geophysical Research*, *104*, 15–24.

Borries, C., Jakowski, N., & Wilken, V. (2009). Storm induced large scale TIDs observed in GPS derived TEC. *Annales Geophysicae*, *27*(4), 1605–1612. https://doi.org/10.5194/angeo-27-1605-2009

Bristow, W. A., Greenwald, R. A., & Samson, J. C. (1994). Identification of high-latitude acoustic gravity waves sources using the Goose Bay HF radar. *Journal of Geophysical Research*, *99*, 319–331. https://doi.org/10.1029/93JA01470

Cai, H. T., Yin, F., Ma, S. Y., & McCrea, I. W. (2011). Observations of AGW/TID propagation across the polar cap: A case study. *Annales Geophysicae*, *29*(8), 1355–1363. https://doi.org/10.5194/angeo-29-1355-2011

Coley, W. R., & Heelis, R. A. (1995). Adaptive identification and characterization of polar ionization patches. *Journal of Geophysical Research*, *100*(A12), 23,819–23,827. https://doi.org/10.1029/95JA02700

Coster, A. J., Goncharenko, L. M., Zhang, S.-R., Erickson, P. J., Rideout, W., & Vierinen, J. (2017). GNSS observations of ionospheric variations during the 21 August 2017 solar eclipse. *Geophyical Research Letters*, *44*, 12,041–12,048. https://doi.org/10.1002/2017GL075774

Cowling, D. H., Webb, H. D., & Yeh, K. C. (1971). Group rays of internal gravity waves in a wind-stratified atmosphere. *Journal of Geophysical Research*, *76*(1), 213–220. https://doi.org/10.1029/JA076i001p00213

Crowley, G., Jones, T. B., & Dudeney, J. R. (1987). Comparison of short period TID morphologies in Antarctica during geomagnetically quiet and active intervals. *Journal of Atmospheric and Terrestrial Physics*, *49*(111-2), 1155–1162. http://doi.org/10.1016/0021-9169(87)90098-5

Deng, Y., Fuller-Rowell, T. J., Akmaev, R. A., & Ridley, A. J. (2011). Impact of the altitudinal Joule heating distribution on the thermosphere. *Journal of Geophysical Research*, *116*, A05313. http://doi.org/10.1029/2010JA016019

Ding, F., Wan, W., Ning, B., & Wang, M. (2007). Large-scale traveling ionospheric disturbances observed by GPS total electron content during the magnetic storm of 29-30 October 2003. *Journal of Geophysical Research*, *112*, A06309. https://doi.org/10.1029/2006JA012013

Fedorenko, A. K., Bespalova, A. V., Cheremnykh, O. K., & Kryuchkov, E. I. (2015). A dominant acoustic-gravity mode in the polar thermosphere. *Annales Geophysicae*, *33*(1), 101–108. https://doi.org/10.5194/angeo-33-101-2015

Ferdousi, B., Nishimura, Y., Maruyama, N., & Lyons, L. R. (2019). Subauroral neutral wind driving and its feedback to SAPS during the 17 March 2013 geomagnetic storm. *Journal of Geophysical Research: Space Physics*, *124*, 2323–2337. https://doi.org/10.1029/2018JA026193

Foster, J. C., & Burke, W. J. (2002). SAPS: A new categorization for sub-auroral electric fields. *Eos, Transactions American Geophysical Union*, *83*(36), 393–394. https://doi.org/10.1029/2002EO000289

Foster, J. C., Erickson, P. J., Coster, A. J., Goldstein, J., & Rich, F. J. (2002). Ionospheric signatures of plasmaspheric tails. *Geophysical Research Letters*, *29*, 1623. https://doi.org/10.1029/2002GL015067

Francis, S. H. (1975). Global propagation of atmospheric gravity waves: A review. *Journal of Atmospheric and Terrestrial Physics*, *37*(6-7), 1011–1054. http://doi.org/10.1016/0021-9169(75)90012-4

Frissell, N. A., Baker, J. B. H., Ruohoniemi, J. M., Gerrard, A. J., Miller, E. S., Marini, J. P., et al. (2014). Climatology of medium-scale traveling ionospheric disturbances observed by the midlatitude Blackstone superDARN radar. *Journal of Geophysical Research: Space Physics*, *119*, 7679–7697. https://doi.org/10.1002/2014JA019870

Fukao, S., Kelley, M. C., Shirakawa, T., Takami, T., Yamamoto, M., Tsuda, T., & Kato, S. (1991). Turbulent upwelling of the midlatitude ionosphere. 1. Observational results by the MU radar. *Journal of Geophysical Research*, *96*(A3), 3725–3746.

Guo, J. P., Deng, Y., Zhang, D. H., Lu, Y., Sheng, C., & Zhang, S.-R. (2018). The effect of subauroral polarization streams on ionosphere and thermosphere during the 2015 St. Patrick's Day Storm: Global ionosphere-thermosphere model simulations. *Journal of Geophysical Research: Space Physics*, *123*, 2241–2256. https://doi.org/10.1002/2017JA024781

Hines, C. O. (1960). Internal atmospheric gravity waves at ionospheric heights. *Canadian Journal of Physics*, *38*(11), 1441–1481. https://doi.org/10.1139/p60-150

Hocke, K., & Schlegel, K. (1996). A review of atmospheric gravity waves and travelling ionospheric disturbances: 1982-1995. *Annales Geophysicae*, *14*(9), 917–940. https://doi.org/10.1007/s00585-996-0917-6

Huang, C. Y., Huang, Y., Su, Y. J., Huang, T., & Sutton, E. K. (2017). High-latitude neutral mass density maxima. *Journal of Geophysical Research: Space Physics*, *122*, 10,694–10,711. https://doi.org/10.1002/2017JA024334

Hunsucker, R. D. (1982). Atmospheric gravity waves generated in the high-latitude ionosphere: A review. *Reviews of Geophysics*, *20*(2), 293–315. https://doi.org/10.1029/RG020i002p00293

Johnson, F. S., Hanson, W. B., Hodges, R. R., Coley, W. R., Carignan, G. R., & Spencer, N. W. (1995). Gravity waves near 300 km over the polar caps. *J. Geophys. Res.*, *100*(A12), 23,993–24,002.

Jonah, O. F., Coster, A., Zhang, S.-R., Goncharenko, L. M., Erickson, P. J., de Paula, E. R., & Kherani, E. A. (2018). TID observations and source analysis during the 2017 Memorial Day Weekend geomagnetic storm over North America. *Journal of Geophysical Research: Space Physics*, *42*, 7874. https://doi.org/10.1029/2018JA025367

Kotake, N., Otsuka, Y., Ogawa, T., Tsugawa, T., & Saito, A. (2007). Statistical study of medium-scale traveling ionospheric disturbances observed with the GPS networks in Southern California. *Earth, Planets and Space*, *59*(2), 95–102. https://doi.org/10.1186/BF03352681

Liu, C. H., & Yeh, K. C. (1969). Effect of ion drag on propagation of acoustic-gravity waves in the atmospheric F region. *Journal of Geophysical Research*, *74*(9), 2248–2255. https://doi.org/10.1029/JA074i009p02248

Lu, G., Hagan, M. E., Häusler, K., Doornbos, E., Bruinsma, S., Anderson, B. J., & Korth, H. (2015). Global ionospheric and thermospheric response to the 5 April 2010 geomagnetic storm: An integrated data-model investigation. *Journal of Geophysical Research: Space Physics*, *119*, 10,358–10,375. https://doi.org/10.1002/2014JA020555

Lühr, H., Rother, M., Köhler, W., Ritter, P., & Grunwaldt, L. (2004). Thermospheric up-welling in the cusp region: Evidence from CHAMP observations. *Geophyical Research Letters*, *31*, L06805. https://doi.org/10.1029/2003GL019314

Lyons, L. R., Nishimura, Y., Zhang, S.-R., Coster, A. J., Bhatt, A., Kendall, E., & Deng, Y. (2019). Identification of auroral zone activity driving large-scale traveling ionospheric disturbances. *Journal of Geophysical Research: Space Physics*, *124*, 700–714. https://doi.org/10.1029/2018JA025980

Makela, J. J., & Otsuka, Y. (2011). Overview of nighttime ionospheric instabilities at low- and mid-latitudes: Coupling aspects resulting in structuring at the mesoscale. *Space Science Reviews*, *168*(1-4), 419–440. https://doi.org/10.1007/s11214-011-9816-6

Nishi, K., Shiokawa, K., & Spence, H. (2018). Magnetospheric source region of auroral finger-like structures observed by the RBSP-A satellite. *Journal of Geophysical Research: Space Physics*, *123*, 7513–7522. https://doi.org/10.1029/2018JA025480

Nishimura, Y., Lyons, L. R., Zou, Y., Oksavik, K., Moen, J. I., Clausen, L. B., et al. (2014). Day-night coupling by a localized flow channel visualized by polar cap patch propagation. *Geophysical Research Letters*, *41*, 3701–3709. https://doi.org/10.1002/2014GL060301

Oinats, A. V., Nishitani, N., Ponomarenko, P., Berngardt, O., & Ratovsky, K. (2016). Statistical characteristics of medium-scale traveling ionospheric disturbances revealed from the Hokkaido East and Ekaterinburg HF radar data. *Earth Planets Space*, *68*, 8. https://doi.org/10.1186/s40623-016-0390-8

Otsuka, Y., Shiokawa, K., Ogawa, T., & Wilkinson, P. (2004). Geomagnetic conjugate observations of medium-scale traveling ionospheric disturbances at midlatitude using all-sky airglow imagers. *Geophysical Research Letters*, *31*, L15803. https://doi.org/10.1029/2004GL020262

Perkins, F. W. (1973). Spread F and ionospheric currents. *Journal of Geophysical Research*, *78*, 218–226.

Ren, J., Zou, S., Gillies, R. G., Donovan, E., & Varney, R. H. (2018). Statistical characteristics of polar cap patches observed by RISR-C. *Journal of Geophysical Research: Space Physics*, *123*, 6981–6995. https://doi.org/10.1029/2018JA025621

Richmond, A. D. (1978). Gravity wave generation, propagation, and dissipation in the thermosphere. *Journal of Geophysical Research*, *83*, 4131–4145. https://doi.org/10.1029/JA083iA09p04131

Rideout, W., & Coster, A. (2006). Automated GPS processing for global total electron content data. *GPS Solutions*, *10*, 219–228. https://doi.org/10.1007/s10291-006-0029-5

Saito, A., Nishimura, M., Yamamoto, M., Fukao, S., Kubota, M., Shiokawa, K., et al. (2001). Traveling ionospheric disturbances detected in the FRONT Campaign. *Geophyical Research Letters*, *28*(4), 689–692. https://doi.org/10.1029/2000GL011884

Savitzky, A., & Golay, M. J. E. (1964). Smoothing and differentiation of data by simplified least squares procedures. *Analytical Chemistry*, *36*, 1627–1639.

Shiokawa, K., Hashimoto, A., Hori, T., Sakaguchi, K., Ogawa, Y., Donovan, E., et al. (2014). Auroral fragmentation into patches. *Journal of Geophysical Research: Space Physics*, *119*, 8249–8261. https://doi.org/10.1002/2014JA020050

Shiokawa, K., Ihara, C., Otsuka, Y., & Ogawa, T. (2003). Statistical study of nighttime medium-scale traveling ionospheric disturbances using midlatitude airglow images. *Journal of Geophysical Research*, *108*, 1052. https://doi.org/10.1029/2002JA009491

Shiokawa, K., Mori, M., Otsuka, Y., Oyama, S., & Nozawa, S. (2012). Motion of high-latitude nighttime medium-scale traveling ionospheric disturbances associated with auroral brightening. *Journal of Geophysical Research*, *117*, A10316. https://doi.org/10.1029/2012JA017928

Tsugawa, T., Otsuka, Y., Coster, A. J., & Saito, A. (2007). Medium-scale traveling ionospheric disturbances detected with dense and wide TEC maps over North America. *Geophyical Research Letters*, *34*, L22101. https://doi.org/10.1029/2007GL031663

Tsugawa, T., Saito, A., & Otsuka, Y. (2004). A statistical study of large-scale traveling ionospheric disturbances using the GPS network in Japan. *Journal of Geophysical Research*, *109*, 669. https://doi.org/10.1029/2003JA010302

Vadas, S. L., & Nicolls, M. J. (2012). The phases and amplitudes of gravity waves propagating and dissipating in the thermosphere: Theory. *Journal of Geophysical Research*, *117*, A05322. http://doi.org/10.1029/2011JA017426

Vierinen, J., Coster, A. J., Rideout, W. C., Erickson, P. J., & Norberg, J. (2016). Statistical framework for estimating GNSS bias. *Atmospheric Measurement Techniques*, *9*, 1303–1312. http://doi.org/10.5194/amt-9-1303-2016

Wang, H., Lühr, H., Häusler, K., & Ritter, P. (2011). Effect of subauroral polarization streams on the thermosphere: A statistical study. *Journal of Geophysical Research*, *116*(A3), A03312. https://doi.org/10.1029/2010JA016236

Wang, W., Talaat, E. R., Burns, A. G., Emery, B., Hsieh, S.-Y., Lei, J., & Xu, J. (2012). Thermosphere and ionosphere response to subauroral polarization streams (SAPS): Model simulations. *Journal of Geophysical Research*, *117*, A07301. http://doi.org/10.1029/2012JA017656

Wu, Q., Jee, G., Lee, C., Kim, J.-H., Kim, Y. H., Ward, W., & Varney, R. H. (2017). First simultaneous multistation observations of the polar cap thermospheric winds. *Journal of Geophysical Research: Space Physics*, *122*, 907–915. https://doi.org/10.1002/2016JA023560

Yeh, K. C., & Liu, C. H. (1974). Acoustic-gravity waves in the upper atmosphere. *Reviews of Geophysics*, *12*(2), 193–216. https://doi.org/10.1029/RG012i002p00193

Yeh, K. C., Webb, H. D., & Cowling, D. H. (1972). Evidence of directional filtering of travelling ionospheric disturbances. *Nature Physical Science*, *235*(59), 131–132. https://doi.org/10.1038/physci235131a0

Zakharenkova, I., Astafyeva, E., & Cherniak, I. (2016). GPS and GLONASS observations of large-scale traveling ionospheric disturbances during the 2015 St. Patrick's Day storm. *Journal of Geophysical Research: Space Physics*, *121*, 12,138–12,156. https://doi.org/10.1002/2016JA023332

Zhang, S.-R., Coster, A. J., Erickson, P. J., Goncharenko, L. P., Rideout, W., & Vierinen, J. (2019). Traveling ionospheric disturbances and ionospheric perturbations associated with solar flares in September 2017. *Journal of Geophysical Research: Space Physics*, *60*, 5894–5917. https://doi.org/10.1029/2019JA026585

Zhang, S.-R., Erickson, P. J., Foster, J. C., Holt, J. M., Coster, A. J., Makela, J. J., et al. (2015). Thermospheric poleward wind surge at midlatitudes during great storm intervals. *Geophyical Research Letters*, *42*, 5132–5140. https://doi.org/10.1002/2015GL064836

Zhang, S.-R., Erickson, P. J., Goncharenko, L. P., Coster, A. J., Rideout, W., & Vierinen, J. (2017). Ionospheric bow waves and perturbations induced by the 21 August 2017 solar eclipse. *Geophyical Research Letters*, *44*, 12,067–12,073. https://doi.org/10.1002/2017GL076054

Zhang, S.-R., Erickson, P. J., Zhang, Y., Wang, W., Huang, C., Coster, A. J., et al. (2017). Observations of ion-neutral coupling associated with strong electrodynamic disturbances during the 2015 St Patrick's Day storm. *Journal of Geophysical Research: Space Physics*, *122*, 1314–1337. https://doi.org/10.1002/2016JA023307

Zhang, Q. H., Zhang, B. C., Lockwood, M., Hu, H. Q., Moen, J., Ruohoniemi, J. M., et al. (2013). Direct observations of the evolution of polar cap ionization patches. *Science*, *339*(6127), 1597–1600. https://doi.org/10.1126/science.1231487